INTERPRETATION OF 2D MAGNETIC ANOMALIES USING THE WAVELET TRANSFORM

© 2025 S. A. Merkuryev*, S. A. Ivanov, I. M. Demina*****

Saint Petersburg Branch of the Institute of Terrestrial Magnetism, Ionosphere and Radio Wave Propagation of the Russian Academy of Sciences (IZMIRAN SPbF), Saint Petersburg, Russia

**e-mail: sam_hg@hotmail.com*

***e-mail: sergei.a.ivanov@mail.ru*

****e-mail: dim@izmiran.spb.ru*

Received May 28, 2024

Revised August 26, 2024

Accepted September 26, 2024

Abstract. Determination of the boundaries of anomaly-forming bodies (deep sources) is an important step in interpreting potential field anomalies during geophysical research. In this paper, a method based on continuous wavelet analysis of magnetic profiles is proposed to solve this problem. The connection between the parameters of simple bodies and the properties of the wavelet transformation of the field created by these bodies is shown. A technique has been developed for determining the boundaries of blocks of the magnetically active layer. The proposed method was tested on model data of the simplest single bodies and on a spreading model. The high resolution of the method is shown, which makes it possible to determine the boundaries of blocks of the spreading model with an accuracy of up to 400 m. The method was applied to a real magnetic profile crossing a typical oceanic structure: the mid-ocean Reykjanes Ridge. The results obtained confirm that the proposed method has a higher resolution compared to the analytical signal and allows the identification of narrow blocks. To clarify the boundaries of these blocks, it is planned to develop a methodology based on the modeling results.

Keywords: *magnetically active layer, block boundaries, wavelet analysis, analytical signal method*

DOI: 10.31857/S00167940250209e4

1. INTRODUCTION

The task of determining the spatial localization and geological structure of potential field sources based on gravimetric and magnetic data has been and remains in the focus of geophysicists'

attention, since its solution is crucial in planning and organizing exploratory and special operations, as well as underlies fundamental and applied research. To solve this problem, there are various techniques for processing geophysical information and signal analysis methods such as Fourier transform, filtering, power spectrum, derivatives, etc., which are widely used in geophysical models for studying Earth structures.

For the analysis of magnetic data, several methods have been proposed that make it possible to interpret the geometry of the sources. Among them, methods based on calculating field derivatives can be distinguished [Miller and Singh, 1994; Verduzco et al., 2004], [Wijns et al., 2005], [Cooper and Cowan, 2006], [Ferreira et al., 2013]. These methods are easy to implement and do not require large computational costs. Their review and comparative analysis can be found in [Gunn, 1997; Nabighian et al., 2005; Cooper and Cowan, 2011].

Another equally important task in interpreting magnetic anomalies is to determine the depth of the source. To solve this problem, automatic methods such as the Werner deconvolution [Werner, 1953] and Euler deconvolution [Thompson, 1982; Reid et al., 1990] have become most popular, in which the problem of depth estimation is transformed into the solution of a system of linear equations. Another approach to obtaining an estimate of the depth of the magnetoactive layer is to use spectral analysis of magnetometric data. In fact, this method is the transformation of a magnetic field from a spatial domain to a frequency domain using a one- or two-dimensional, depending on the type of initial magnetic data, Fourier transform with its subsequent interpretation. The method proposed in [Spector and Grant, 1970] was widely used, where an ensemble of blocks of various depths, widths, thicknesses, and magnetization was considered as a model of anomaly-forming bodies, and the shape of the magnetic data spectrum was analyzed depending on these parameters. The possibility of determining the power of a magnetically active layer by autocorrelation functions was considered in [Portnova et al., 1987].

The methods listed above are usually used for the primary analysis of area data (grids) in the study of Earth structures, since they allow you to quickly get a qualitative idea of the main features of the studied regions, with minimal a priori representations. Obtaining quantitative characteristics for more complex bodies and models requires the use of more sophisticated methods and interpretation schemes.

The analytical signal method is well known and widely used to identify the boundaries of anomaly-forming bodies [Nabighian, 1972; Nabighian, 1974]. The popularity of this method is due to the fact that its application does not impose any restrictions on the shape of the desired source. The main advantage of the analytical signal is that for two-dimensional magnetic sources, the shape and location of its amplitude maxima do not depend on the direction of magnetization [MacLeod et al., 1993]. This property ensured its wide application for the interpretation of marine magnetic

anomalies due to its independence from the direction of the ancient and modern fields, which eliminated the need to take into account the obliquity of anomalies when determining the location of vertical boundaries between blocks of opposite magnetic polarity, for example, [Roest, et al., 1992].

However, it has been shown that the shape of the analytical signal of the magnetic field of a dipole or spherical source depends on the direction of magnetization, and its amplitude peaks are not always located directly above such sources, their displacement depends on the source-observation distance and the shift can be up to 30% of the distance [Salem et al., 2002].

Previously, we investigated the resolution of the analytical signal method [Ivanov and Merkuryev, 2014] and, using the simplest example of a vertical dike, numerically and analytically demonstrated the difficulties of determining the position of the source with large ratios of depth and width of the source.

In recent years, the wavelet transform has become widespread in signal analysis. The fundamentals of the theory of the wavelet transform and examples of its use are given in domestic and foreign reviews [Astafieva, 1996; Moreau et al., 1977, Kumar, Foufoula-Georgiou, 1997]. The wavelet transform, like the Fourier transform and any other integral transform, inherits the properties of the analyzed function and the basic kernel [Glaznev, 2003]. But unlike the Fourier transform, in which the analyzing function covers the entire time axis, the two-parameter generating function of the one-dimensional wavelet transform is well localized in both time and frequency. This property allows us to obtain more information about the signal, but the interpretation of the wavelet spectrum is not as obvious as the analysis of the Fourier transform. Various schemes for interpreting geophysical data using different types of wavelet transform are proposed: for example, in [Obolensky and Bulychev, 2011; Kuznetsov and Bulychev, 2017] proposed the use of complex Poisson wavelets of arbitrary order. The results of the wavelet analysis of ground-based, aeromagnetic, and balloon surveys in the area of the Kursk magnetic anomaly are described in [Ivanov et al., 2002]. Gaussian wavelets are studied in detail in [Khvastunov, 1998]. In [Glaznev and Muravina 2020], the properties of a Mexican hat wavelet were considered and it was proposed to use the solution of a direct problem for this type of body as a mother function. The work [Sailhac et al., 2000] shows how to use complex wavelets to interpret aeromagnetic data.

We have previously conducted a study of errors and limitations that occur on models of bodies of simple shape and proposed methods to reduce the error rate. The interpretation of magnetic anomalies over bodies of simple shape is considered in the extensive geological and geophysical literature on exploration geophysics, see, for example, [Gay, 1963; Zakharov and Logachev, 1979], since the shape of these bodies accounts for a significant percentage of known geological and mineral manifestations (dikes, veins, faults, contacts and layered rocks). In addition,

simple-shaped bodies and their combinations underlie more complex models used in solving fundamental geophysics problems, one of which is the interpretation of marine magnetic anomalies. The developed methodological approaches were tested on a spreading model, and then applied to a real magnetometric profile crossing the Reykjavik Ridge. We compared the results of the wavelet analysis on model and real data with the results of using the analytical signal method.

2. APPLYING THE WAVELET TRANSFORM TO MODEL FIELDS

The wavelet transform W of the original signal f with respect to the wavelet function ψ is expressed by the formula

$$W(a,b) = \frac{1}{|a|^{1/2}} \int_{-\infty}^{\infty} f(x)\psi^*\left(\frac{x-b}{a}\right) dx,$$

where f(x) is the analyzed signal, a is the wavelet scale, b is the shift, and ψ is the generating function. Due to a, the size of the segment of the generating function assignment changes, and b sets the localization of the generating function along the analyzed signal. One of the most important properties of wavelets is that they provide time-frequency localization of the structural features of the analyzed signal and allow tracking their change over time.

To date, a large number of families of wavelets have been developed based on various functions with a wide range of properties that determine their application in a particular task. For example, those wavelet families that have an inverse transformation are often used to filter signals (see, for example, [Voskoboinikov, 2015]). The continuous Morley wavelet is useful for analyzing the spectral composition and its changes over time. Our task is to localize the features of the original signal related to the structural inhomogeneities of its source. In [Kuznetsov and Bulychev 2017; Obolensky and Bulychev 2011; Kuznetsov et al., 2015], a complex Poisson wavelet was used for this purpose. In this paper, we propose using a family of wavelets based on derivatives of the Gauss function, expressed up to a constant as

$$\psi(x) = (-1)^{m-1} \frac{d}{dx^m}\left[exp\left(\frac{-x^2}{2}\right)\right],$$

where m is the order of the derivative. The choice of this wavelet is based on the task of interpreting marine magnetic anomalies, which consists in localizing the boundaries of oceanic crust blocks with different magnetization, which is precisely provided by the selected family of wavelets. Indeed, a detailed analysis of the properties of wavelets based on derivatives of the Gauss function [Khvastunov, 2002] showed that for a signal similar in shape to the Gauss function, the extremes of its wavelet spectrum calculated at different m coincide with the extremes of the corresponding signal derivatives. We used wavelets with m = 1,2,3. Modulo the wavelet coefficients, the coordinates of

the local maxima are determined for each scale, which form vertical lines parallel to the axes of the scales. At the first stage, we applied this approach to analyzing the field of simple geological formations.

2.1. Bodies of simple shape

The most important property of the wavelet transform using derivatives of the Gauss function for the interpretation of magnetic anomalies is that the coordinates of the extremes of these wavelets coincide with the coordinates of the extremes of the corresponding derivatives of the observed field. These extremes are determined by the properties of a geological object, and in the case where analytical expressions can be obtained for these points, all its parameters can be found using the coordinates of the extremes of the wavelet spectra and assuming the shape of the body. For a set of bodies of simple shape, we have obtained the corresponding formulas that can be used to construct equations for geometric parameters (all necessary formulas are given in the Appendix). We show this by using the example of several bodies of simple shape. The paper considers only linear structures of infinite extension along the y coordinate. The cross sections of the bodies under consideration are shown in Fig. 1.

2.1.1. Quadrant

A configuration that can be considered as the main element in the geometry of any body with rectangular borders parallel to the coordinate axes is a body with a section in the form of a quadrant with a vertex at (x0, z1) (see Fig. 1a). The field created by this object is determined by the formula [Talwani, Heirtzler, 1964]

$$B_z = \text{arctg}((x - x_0)/z_1).$$

Here and everywhere else, we omit the dimensional factors related to the magnitude of the magnetization. This model can be applied to bodies whose vertices (cross-section angles) are spaced by a considerable distance. In general, the proposed methods work better the closer the field in the vicinity of the vertex is to the field of the quadrant.

Using the wavelet spectrum, we can determine the position of the extrema of the derivatives of different orders. The quadrant has two parameters: x0 is the coordinate of the corner point of the section and z1 is the depth to the upper edge (hereinafter, just the depth). According to (N1), the extremum of the first derivative is reached at the angular point x0 . And two extremes of the second derivative with coordinates x± =x0±□3/3z1 (N2) allow us to estimate the depth of z1. The third derivative has three extremes: the central one coincides with the position of the corner point, and the distance from the two lateral ones to the center is equal to the depth (N3). An example of determining the parameters of a quadrant with the specified parameters x0 = 2 km and z1 = 3 km is shown in Fig.

2. In Figure 2, the x-coordinate is set in km, the scales are recalculated in km, and the isolines of the modules of the wavelet coefficients for the three derivatives are shown in solid lines. For each derivative, the coordinates of the local maxima are indicated by points. It is clearly visible that these points line up in straight lines parallel to the axes of scales. The parameters of the quadrant were determined by the intersections of these lines with the x-axis. As a result, the value of x0 = 2.01 km is obtained for the 1st derivative (N1) (Fig. 2a), for the 2nd derivative (N2) – x0 = 2.005 km and z1 = 3.003km (Fig. 2b), for the 3rd derivative (N3) - x0 = 2.0 km and z1 = 3.01 km. (Fig. 2b).

The accuracy of determining the x coordinate of the vertex of a quadrant is practically independent of its depth. So, in the model example, the depth varied from 0.5 to 4 km, while the coordinate of the angle x0 was determined with an error of no more than the field setting step. The depths obtained from the extremes of the 2nd and 3rd derivatives coincide with the accuracy of the first meters.

2.1.2. Semi-infinite horizontal reservoir

The simplest body derived from the quadrant can be considered a semi-infinite horizontal layer (see Fig. 1b). Such a body can be considered composed of two quadrants with magnetization of different signs, and it is described by 3 parameters: 2 coordinates of the upper angular point (x0 and z1) and thickness h=z2-z1. The field created by such a body is expressed by the formula [Nikitsky, Glebovsky, 1990]

$$B_z = \text{arctg}((x - x_0)/z_1) - \text{arctg}\,((x - x_0)/z_2).$$

One of the extrema of the 1st derivative coincides with x0 (the coordinate of the corner point). The other two extrema x_±^1 (here the lower indices are the roots and the upper one is the order of the derivative) are determined by the zeros of the 2nd derivative (N4).

Numerical experiments have shown that the error in determining the x0 coordinates for all derivatives, as in the case of a quadrant, does not exceed 10 m, regardless of thickness. As for the depth and thickness of the formation, in extreme cases when z2"z1 the problem is reduced to the previous one, and the coordinates of the additional extremes tend to ∞. We can find an estimate of the depth of z1 by the extremum of the 3rd derivative, assuming that in the case of the formation the formula (N3) for the quadrant is applicable. Then, knowing the position of the extrema of the 1st derivative x_±1, we obtain the equation for determining z2 (N5). The possibility of using this technique to determine reservoir parameters has been investigated empirically. Calculations were performed for three values of depth z1 and eight values of thickness h. The results are shown in Fig. 3. Figure 3a shows in different symbols the dependence of the depth determination error on the thickness of the formation (from 0.5 km to 8 km). It was found that at a depth of 1 km, this error depends little on the thickness of the formation and does not exceed 200 m in absolute value. But as the depth increases, the thickness of the formation has a decisive influence on the error in determining

the depth. For a depth of 4 km and a thickness of 0.5 km, the error is already 940 m. The error in determining the thickness of the formation is shown in Fig. 3b. The symbols show the dependence on the depth of the formation. It is clearly seen that for a depth of 1 km ( ), the error in determining the thickness depends little on the specified thickness of the formation and does not exceed 200 m. At the same time, for a thin layer, the error increases rapidly with depth and amounts to 1200 m for z= 4 km ( ). If we go to dimensionless units, dividing both the thickness and the error of its determination by the depth (Fig. 3b), we obtain that the relative error depends only on the relative depth and is negligible for h/z1≫1.

2.1.3. Dike

A dike or vertical seam of a given width is also characterized by three parameters: center x0, half-width d, and depth z1 to the upper edge (see Fig. 1b). The section S has the form S = {x0-d<x< x0+d, z < −z1}. The field created by such a body is expressed by the formula [Nikitsky, Glebovsky, 1990]

$$B_z = \text{arctg}\left(\frac{x - x_0 - d}{z_1}\right) - \text{arctg}\left(\frac{x - x_0 + d}{z_1}\right)$$

This type of geological object is especially important for us when looking for excursions into the structure of marine magnetic anomalies. For dyke, only the extremes of the 1st derivative (N6) can be obtained analytically. Which gives the position of the center. If we consider a dike as a combination of two separated quadrants, then the coordinates of its corner points can be determined by the position of the extrema of the 1st and 3rd derivatives, which gives a half-width. Then the depth can be calculated from (N6). In the case of dyke, the extremes of the 3rd derivative give more accurate values of the coordinates of the corner points. It should be noted that the depth of the magnetoactive layer in the case of interpretation of marine magnetometric data can often be obtained from bathymetry.

An important question for interpretation has been empirically investigated: at what width of the dike is the error in determining its parameters in the same way as for the quadrant negligible. By changing the half-width and depth of the dike and determining the extremum points of the 1st and 3rd derivatives, we obtain estimates of the values of the desired parameters. In other words, we assume that

a) the extremes of the 1st and 3rd derivatives correspond to the angular points of dyke.

b) the extremes of the 3rd derivative determine its depth according to the formula (N3) for the quadrant.

The dike width took values of 0.5, 1, 1.5, and 2 km, and the depth varied from 1 to 8 km. Errors in determining the parameters of the dyke for all possible combinations of the set parameters are

shown in Fig. 4a and 4b. An important aspect is that only narrow bodies were considered. It can be seen that the depth estimated from the extremes of the 3rd derivative (Fig. 4a) is somewhat overestimated, but practically does not depend on the width of the dyke. At the same time, the error in determining the half-width (Fig. 4b) increases rapidly with increasing depth. Only when the half-width is twice as large as the depth does the error become small. This is due to the fact that the coordinates of the extremes of both the 1st and 3rd derivatives found in the wavelet spectrum for the dyke do not coincide with its angular points, as was the case for the quadrant, and the discrepancy increases with increasing depth. With a large depth, the dike appears to be much wider than it actually is. However, the position of the center is determined with a small error, as in the cases of the corner points of the quadrant and the formation.

To clarify the value of the dyke half-width d, we can use an explicit expression for the coordinates x_±1 of the extremes of its 1st derivative (N6). At the same time, we assume that z1 and x0 are known. After simple transformations from (N6), we obtain the formula for determining the half-width. Denoting x_±^1 x0≡q, we write the equation for the half-width as

$$d = \sqrt{2q\sqrt{q^2 + z_1^2} - q^2 - z_1^2} \qquad (1)$$

It follows from this formula that the distance of the extremum to the center of x0 is greater than the half-width. If the depth is less than half the width, ε = z1/d<1, then formula (1) can be approximately written as d = q(1-ε4/8). If the value of z1 is known from independent sources, using formula (1) it is possible to obtain half-width values with an error not exceeding one hundred meters in the most unfavorable case of a deep narrow dike. However, if the values of z1 were determined from the extremes of the 3rd derivative (Fig. 4a), the error increases dramatically, moreover, in some cases imaginary values are obtained as a half-width.

Estimates of the half-width and depth for dikes can be obtained more accurately if the task is complicated and the extremes of the 2nd derivative are used to determine them. In this case, we obtain a system of two equations with two unknowns d and z1, and we consider x0 to be known. To obtain the first equation, the 2nd derivative (N7) was equated to zero for x equal to the found extremum of the 1st derivative (N6). To obtain the second equation, the 3rd derivative (N8) was equated to zero for x equal to the found extremum of the 2nd derivative (for simplicity, the dyke center has a zero coordinate in the formula). We solved the system numerically. The values of depths and half-widths obtained from the solution of the system are shown in Fig. 4b and 4g. It can be seen that when using this approach, the error can be reduced several times. However, in some cases, the solution of the system is unstable and requires precise determination of the position of the extremes, which directly

depends on the step of setting the initial signal. In the case of the considered model, knowledge of the initial signal with a step of several meters was required for large depths.

Earlier in [Ivanov and Merkuryev, 2014], the problem of determining the parameters of a dyke using the analytical signal method was considered. Using the example of dyke, this allows us to compare the interpretative capabilities of two methods: wavelet analysis and the analytical signal method. For comparison, we present the results of determining the half-width of a dyke to dimensionless units, dividing both the half-width and the error in determining it by the depth of the dyke. Figure 5 shows the result obtained experimentally for the above values of the dyke parameters and using the 1st (triangles) and 3rd (circles) derivatives. For an adequate comparison, the theoretical dependence of the relative error of the wavelet analysis was calculated using the 1st derivative. In Fig. 5, it is shown as a solid line. A similar curve for the analytical signal method is shown in Figure 5 as a dotted line. The theoretical curves for the 3rd derivative were not calculated due to the lack of analytical expressions for the position of the extremes. These results clearly demonstrate that in the case of dyke, the wavelet analysis gives a lower error in determining the parameters compared to the analytical signal method. In addition, the advantage of using the 3rd derivative to determine the half-width of the dike is clearly visible compared to the 1st.

2.2. The three-block model

We propose to use wavelet analysis to interpret marine magnetic anomalies. Since the magnetically active layer of the oceanic crust can be represented as a sequence of blocks (Fig. 1g) of infinite extension in one direction, having a rectangular cross-section in the perpendicular direction, differing in magnetization, we have previously considered a model consisting of three blocks. Such a model can be considered as a combination of simple bodies with the feature that the presence of neighboring sources is an obstacle that can have a significant impact on the result of interpretation using the methods discussed above. The resulting parameter estimation errors and possible methods of reducing them require separate consideration.

Let us consider as a model three consecutive blocks located at the same depth z1 = 3km, having a thickness of h = 0.4 km, differing in half-width and magnetization. Let's put the half-widths d equal to 4.5, 0.5 and 5 km. Such a model can be considered as an element of the oceanic magnetically active layer. The field created by this model and its derivatives are shown in Fig. 6.

Figure 6 in block (a) shows the specified structure of the magnetically active layer. The analysis of the wavelet spectra showed that the depth estimates to the upper edge for all blocks are underestimated and range from 2.7 to 2.85 km. This result is determined by the low layer thickness and corresponds to the estimates obtained earlier for the layer model. The best match with the boundaries can be extracted from the position of the extrema of the 3rd derivative. The result is shown

in Fig. 6 in block (b), while it is clearly visible that the narrow block appears to be widened. This result corresponds to the one obtained above for a narrow dike. It was also shown there that it is possible to refine the half-width based on formula (1). The parameter in this formula is the position of the center point x0. There are 3 ways to estimate the position of the block centers: by the position of the field extremes and by the distance between the boundaries determined by the 1st and 3rd derivatives. The results are presented in Table 1.

You can see that the position of the center of the small block is determined with a small error in any way. For large blocks, determining the center from the extremes of the field and the 3rd derivative give similar results. Next, we used the positions of the centers obtained from the extremes of the 3rd derivative, and estimated the half-widths of the blocks from them. The values of the given half-widths and those obtained from the wavelet spectrum are shown in Table 2 in the corresponding rows. Obviously, correction is required not only for a narrow block. To solve this problem, we will apply the technique described above for the dyke. We will assume that the depth to the upper edge is known, and we will take the coordinates obtained from the 3rd derivative as the positions of the centers. Then, applying formula (1) and solving the resulting equations, we calculate the new values of the half-widths of the blocks (step 1). The results obtained in Step 1 are shown in Table 2.

It is easy to make sure that for each contact, the sum of the half-width values obtained after step 1 is less than the sum of the distances between the centers of each pair of bodies. Obviously, the shift of the extremes towards large bodies leads to the fact that the estimates of their centers are shifted towards opposite boundaries, which, in turn, leads to their underestimated sizes and the observed difference between the sums of the half-widths and the distances between the centers of the bodies. To correct the solution, an algorithm is proposed that assumes varying the position of the centers of large blocks and varying the position of the extremes of the 1st derivative of the central block, followed by using formula (1). The positions of the centers obtained as a result of the above process are shown in Table 1, and the changes in the half-widths are shown in Table 2 in the "After correction" rows. The resulting block configuration is shown in Fig.6b.

The interpretation of the field of the 3-block model showed that the narrow block stands out from the larger ones, and its half-width is greatly overestimated. Using formula (1) alone, it is not possible to restore the positions of the block centers and their half-widths. However, using the procedure of minimizing the discrepancy between the distances between the centers and the sum of the half-widths of the blocks for each contact, it is possible to reduce errors in the initial estimates of the block parameters. The resulting variational problem requires a separate study, but the result suggests that this approach can be applied to interpret real data. It should be noted that the above estimates of errors in determining the parameters of bodies based on the extremes of the wavelet spectra are estimates from below; for real data, the errors may be greater.

3. APPLICATION OF WAVELETANALYSIS TO THE INTERPRETATION OF OCEANIC MAGNETIC ANOMALIES

Due to its nature, the magnetic field of the oceanic crust differs significantly from the field of the continental crust. According to modern concepts, the magnetically active layer responsible for oceanic magnetic anomalies is associated with the inversion-spreading mechanism of its formation on the axes of mid-oceanic ridges, which are a chain of active volcanoes. Igneous rocks erupted on the ocean floor as a result of cooling acquire the thermally sufficient magnetization of the epoch of geomagnetic polarity when this event occurred. Analysis of the structure of the magnetic anomalies that occur in this case allows us to draw conclusions about geological processes that took place tens and hundreds of millions of years ago. The main task in analyzing the oceanic field is to determine the boundaries of blocks of different magnetization, identify and determine the age of the corresponding anomaly.

The theoretical issues of the possibility of resolving oceanic magnetic anomalies using the analytical signal method were discussed earlier in a number of articles [Ivanov and Merkuryev, 2014; Ivanov and Merkuryev, 2016], where, using the simplest example of a vertical dike, it was analytically and numerically shown at what ratios of the depth and width of the source it is difficult to determine its position.

In this paper, we used the wavelet transform for analysis, the applicability of which to the interpretation of magnetic fields was tested on simple geological structures. The results are given above in this paper. Since the application of wavelet analysis to the class of oceanic magnetic anomalies cannot be analytically investigated, we first performed numerical testing of this method using a model example, and then using the example of a typical magnetometric profile on the mid-oceanic ridge.

In this section, we present a comparison of the results of determining the boundaries (edges) of anomaly sources (anomaly-forming bodies) for the spreading model using the analytical signal and wavelet analysis method.

3.1. The analytical signal and its properties

Let us recall the definition and basic properties of an analytical signal.

The analytical signal is defined as the square root of the sum of the squares of the vertical and two horizontal derivatives of the magnetic field anomalies ΔT [Roest et al., 1992].

$$|AS| = \sqrt{\left(\frac{\Delta T}{\partial x}\right)^2 + \left(\frac{\Delta T}{\partial y}\right)^2 + \left(\frac{\Delta T}{\partial z}\right)^2},$$

Here, the z derivative is the Hilbert transform of horizontal derivatives [Nabighian, 1972], which makes it possible to construct an analytical signal module |AS(x,y)| based on a given magnetic anomaly ΔT(x,y).

The analytical signal method is useful for determining the location of vertical boundaries between blocks of opposite magnetic polarity on the oceanic crust, for example, [Roest, et al., 1992]. According to some authors, this method is much more reliable and objective than the traditional method of selection by visual comparison of observed and synthetic anomaly models [Chaubey, 2002]. According to the experience of other researchers, the method did not improve the ability to identify chrones of different polarities; the complex geometry and rotation of magnetized bodies in the axial zone of the slow-spreading ridge are cited as a possible reason [Parnell-Turner et al., 2016].

The algorithm and program used to calculate the spreading model and the analytical signal used the fast Fourier transform [Troshkov and Shalaev, 1961; Schouten and McCamy, 1972], which contributed to the speed of calculations.

3.2. A test case for the spreading model

As a model profile, we used magnetic anomalies calculated using the so-called spreading model, which is widely used in the analysis and interpretation of the oceanic magnetic field. This model is based on a property. high linearity of the structure of oceanic magnetic anomalies. The usual spreading model is a set of infinite blocks of forward and reverse polarity in accordance with the part of the time scale of inversions that accounts for the spreading of the oceanic day in the region under consideration. The horizontal size of the blocks is determined by the spreading rate at which the ocean floor expanded. The depth of the ocean plus the thickness of the sedimentary layer is taken as the depth of the sources.

The spreading model is one of the most complex objects of research, the purpose of which is to determine the position of the boundaries of the blocks that make up the magnetically active layer. The difficulties that arise are related to a number of reasons. The fact is that the length of magnetometric profiles, as a rule, is several hundred kilometers, and the number of direct polarity blocks that make up the magnetically active layer can reach several dozen. The magnetic field is usually recorded by magnetometers towed on the ocean surface, and the magnetoactive layer lies at depths of several kilometers. Therefore, according to the principle of superposition, at each point of the profile we observe the total field of a number of remote sources. It is not always possible to reconstruct the structure of sources from magnetic anomalies, especially if their horizontal size is significantly less than the depth of occurrence.

In this paper, as a test example, we calculated the theoretical magnetic profile from the spreading model, which we previously used in the geochronological analysis of magnetic anomalies

formed on the boundary of the North American and Eurasian plates over the past 20 million years [Merkouriev and DeMets, 2008]. In the calculation, we used the time scale of inversions [Gradstein et al., 2020], the total spreading rate is 20 mm/year, the layer thickness is 0.4 km, and the depth of the upper edge of the layer is 2 km. Figure 7a shows the structure of the magnetoactive layer in the form of blocks of forward and reverse polarity. The blocks of direct polarity are filled in, the boundaries of the chrones are marked, which must be determined by magnetic anomalies using wavelet analysis. The solid line shows a graph of theoretical magnetic anomalies calculated from this magnetically active layer.

A wavelet analysis with a generative function, which is the 3rd derivative of the Gauss function, was applied to this profile. At the same time, an analytical signal analysis was performed for comparison. Figure 7b shows a graph of the analytical signal module calculated from magnetic anomalies. The local maxima of the analytical signal, according to its properties, are located above or near the boundaries of the anomaly-forming bodies. The result of the wavelet analysis is shown in Fig. 7g. The solid lines show the isolines of the wavelet coefficient module, the dots show the local maxima on each scale, the scales are recalculated in km. The comparison of the obtained results is placed in the central block (b). The model scale is repeated here, long vertical segments show the positions of the extremes of the 3rd derivative of the wavelet transform, inverted triangles mark the extremes closest to the desired chronon boundaries, triangles mark the boundaries themselves, and short segments with a diamond show the boundaries defined by using the analytical signal method.

As can be seen from Fig.7b, there is a pretty good correspondence between the desired and found boundaries by both methods. Numerical estimates of the deviation of the found coordinates from the desired coordinates show that the modulus of the average deviation given by the wavelet analysis is 0.33 km, whereas this value for the analytical signal method is 1.2 km. In addition, using the analytical signal, a significantly smaller number of block boundaries were identified and, in particular, it was not possible to determine the boundary of chron 4n.1, whereas with the help of wavelet analysis, the boundaries of all the desired chrones were determined.

3.3. An example of using wavelet analysis on a real magnetometric profile crossing the Reykjavik Ridge

We applied the methodology described above to real data to determine the boundaries of blocks of anomaly-forming bodies according to the magnetometric profile crossing the mid-oceanic ridge (the Reykjavik Ridge). Such a task is typical when conducting geohistorical and kinematic analysis of an anomalous magnetic field, when using magnetic anomalies it is necessary to determine the boundaries of chrones of the same age located on both sides of the axis of the ridge for their subsequent alignment in order to determine the kinematic parameters of rotation of the lithospheric

plates. The KNOR24 profile crossing the Reykjavik Range, located in the North Atlantic Ocean south of Iceland, was chosen as such a profile (Fig. 8). In order to present the geological situation of this region, we recall that the Reykjavik range is a divergent boundary of the North American and Eurasian plates, which diverge at a full spreading rate of about 20 mm/the year [Merkouriev and DeMets, 2008].

The Reykjavik ridge is characterized by high-intensity anomalies with an amplitude of 300-800 NT, and a high-intensity axial anomaly with an amplitude of up to 2500 NT, confined to the axis of the ridge (Fig. 8b). The relief of the ocean floor is quite rugged, especially in the axial zone of the ridge, which is a graben with a depth of about 1000 m and a width of about 70 km, which turns into a gently sloping relief typical of the slopes of Mid-Oceanic ridges (Fig. 8a).

Figure 8b shows a shadow map of the bottom relief with the isochron positions taken out and a graph of the observed magnetic anomalies on the KNOR24 magnetometric profile obtained from the NGDC database [Hey, 2013]. The isochrons shown in Figure 8b with various markers were obtained by us during the study of magnetometric data on the boundary of the North American and Eurasian plates in order to build a high-resolution kinematic model [Merkouriev and DeMets, 2008]. In total, the boundaries of 21 inversions were digitized in the age range of 0.72–20 million years (anomalies 1n – 6n), the average interval between chrones was 1 million years. The anomalies were digitized manually using a program that made it possible to visually compare the model and the observed profile to select a point on the graph corresponding to the position (boundary) of each chron. Note that the point corresponding to the chrono boundary for each anomaly does not always fall on the section of the graph intersecting the horizontal zero axis or at the point of the maximum gradient of the field graph, therefore, digitization of anomalies cannot always be reduced to a formal procedure that can be programmed.

Using the wavelet analysis and the analytical signal method, the boundaries of the anomaly-forming bodies were determined according to the method described above. The results of the analysis of real data are shown in Fig. 9, which is constructed in the same way as Fig. 7. The graph of the analyzed magnetic profile is shown in Fig. 9a, which contains the boundaries of the chrones that we digitized manually [Merkouriev and DeMets, 2008; DeMets and Merkouriev, 2020]. We consider the position of these chrones as the desired source boundaries, which must be determined using wavelet analysis and the analytical signal method. The same block below shows the magnetically active layer of the spreading model that we used earlier for testing. Recall that we calculated the spreading model at a constant spreading rate of 20 mm/year, and the scale shown here serves to be able to compare the chrones digitized on the observed profile with the corresponding chrones on the scale.

Figure 9b shows a graph of the amplitude of the analytical signal calculated from the magnetic anomalies observed on the KNOR24 profile. The boundaries of the sources were determined from

the local maxima of the analytical signal, which are shown as black segments with diamonds in Fig.9b. The boundaries determined from the local maxima found using wavelet analysis with a generating function - the 3rd derivative of the Gaussian function (Fig. 9g) are shown in Fig. 9 with inverted triangles inside. In the same drawing, the up marker shows the desired chrono boundaries.

As can be seen from Fig.9b, as well as for the spreading model, there is a pretty good correspondence between the desired and found boundaries obtained using wavelet analysis. The numerical estimates of the modulus of deviation of the found coordinates from the desired ones obtained for the real profile were 0.25 ± 0.2 km for the wavelet analysis, whereas for the analytical signal method it was 1.5 ± 1.1 km.

4. CONCLUSION

In this paper, it is proposed to use the wavelet transform with generating functions representing derivatives of the Gauss function of 1-3 orders for the interpretation of magnetic anomalies.

The possibilities and limitations of the method are investigated on models of the simplest linear structures, infinite extension along one coordinate with a section in the form of a quadrant, formation and dyke.

1. Working formulas are given that relate the position of the extremes of the derivatives of the magnetic fields of these linear structures to their parameters.

2. It is shown that using the positions of the extrema of the wavelet transform with derivatives of the Gaussian function of different orders, it is possible to determine the geometric parameters of the above bodies of simple shape.

3. An analysis of the errors that occur is carried out and estimates of the accuracy of the results are given.

4. It is shown numerically that the wavelet transform makes it possible to determine the coordinates of contacts more precisely, the closer the fields in the vicinity of the contact are to the field of a body with a quadrant section.

5. Methods for clarifying the parameters of bodies using a combination of wavelet transformations with derivatives of different orders from the Gauss function are proposed. It is shown that the problem is reduced to solving a system of equations, the degree of which depends on the order of the derivatives. At the same time, to ensure the stability of the resulting solution, greater accuracy is required in determining the coordinates of the extremes of the wavelet spectrum.

6. Using the example of determining dyke parameters analytically and numerically, it is shown that the wavelet transform gives a lower error in determining the parameters compared to the analytical signal method.

7. As an example of a multi-body structure, a model with a cross-section in the form of 3 blocks is considered in detail. It is found that if a narrow block is present in the model, the wavelet transform makes it possible to establish its presence in the structure. Clarifying the coordinates of the boundaries and widths of the blocks requires additional methodological developments.

8. The efficiency of the method is shown using the example of the Vine-Matthews model, which covers the last 20 million years. Numerical estimates have shown that the modulus of the average deviation of the found coordinates of the chronon boundaries from those sought by the wavelet analysis is 0.33 km, whereas this value for the analytical signal method is 1.2 km. In addition, using the analytical signal method, a significantly smaller number of block boundaries were identified, whereas using wavelet analysis, the boundaries of all the desired chrones were determined.

9. The method is applied to the data of a real profile crossing the Reykjavik ridge, and it is found that the numerical estimates of the average deviations of the chrono coordinates from the wavelet analysis are 0.25±0.2 km, whereas this value for the analytical signal method is 1.5±1.1 km. This showed the advantage of the wavelet transform method over the analytical signal method in the task of determining contacts for real data.

FUNDING

The work was carried out within the state budget.

CONFLICT OF INTERESTS

The authors declare that there is no conflict of interest.

REFERENCES

1. *Astafyeva N.M.* Wavelet analysis: fundamentals of theory and application examples / / UFN. T. 166. № 11. pp. 1145-1170. 1996.
2. *Voskoboinikov Yu.E.* Wavelet filtering of signals and images (with examples in theMphCAD package). НовосибNovosibirsk State University of Architecture.- builds. un-t (Sibstrin). Novosibirsk: NGASU (Sibstrin). 188 p. 2015.
3. *Zakharov V.P., Logachev A.A.* Magnetorazvedka. Izd. 2. L.: Nedra. 351 p. 1979.
4. *Ivanov, V.V., Rotanova, N.M., Kovalevskaya, E.V., and Tsvetkov, Yu.P.*, Using the results of wavelet analysis to estimate the depth of magnetic sources, Geomagnetism and Aeronomy, vol. 42, No. 4, pp. 569-576, 2002.

5. *Ivanov S.A.,* Merkur *'ev S.A.* Interpretation of marine magnetic anomalies. Part 1. Review of existing methods and analysis of the analytical signal method / / Geomagnetism and Aeronomy, vol. 54, No. 3, pp. 420-428.
2014.. https://doi.org/10.7868/S0016794014030080
6. *Ivanov S.A., Merkur'ev S.A.* Possibilities of paleomagnetic and geohistorical analysis of short-period marine magnetic anomalies of the “tiny wiggles”type // Geomagnetism and Aeronomy, vol. 56, No. 3, pp. 393–406. 393-406, 2016.
https://doi.org/10.7868/S0016794016030081.org/10.7868/S0016794016030081
7. *Glaznev V.N.* Complex geophysical models of the Fennoscandia lithosphere. // Apatity. "KaeM". 252 p. 2003.
8. *Glaznev V.N., Muravina O.M.* Using wavelet transforms for analysis and interpretation of potential fields. / Questions of theory and practice of geological interpretation of geophysical fields. Proceedings of the 47th session of the International Scientific Seminar D.G. Uspensky - V.N. Strakhov. Voronezh: CPI "Nauchnaya kniga" 2020. pp. 89-93.
9. *Kuznetsov K.M., Bulychev A.A.* Poisson wavelets in problems of processing areal potential fields // Vestn. KRAUNTS. Ser.: Earth Sciences. Issue36, No. 4, pp. 72-78 , 2017.
10. *Kuznetsov K.M., Obolensky I.V., Bulychev A.A.* Potential field transformations based on continuous wavelet transform // Vestn. MSU. Ser. 4.Geologiya [Geology]. No. 6. pp. 61-70, 2015.
11. *Nikitsky V.E., Glebovsky Yu.S.* Magnetorazvedka [Magnetorazvedka], Ed. 2, Moscow: Nedra. 470 p. 1990.
12. *Obolenskiy, I.V. and Bulychev, A.A.*, Application of the complex continuous Poisson wavelet transform to determine the sources of potential field anomalies, Geofizich. research, vol. 12, No. 3, pp. 5-21, 2011.
13. *Troshkov, G.A. and Shalaev, S.V.*, Application of the Fourier transform to solve the inverse problem of gravity and magnetic exploration, Prikladnaya geofizika. Issue30, pp.–178. 162-178, 1961.
14. *Khvastunov M.S.* Wavelet analysis: application to Gaussian form signals. // JINR Rapid Comm. Vol. 92. no. 6. pp.63-74. 1998.
15. *Catalán M, Martos Y.M., Galindo-Zaldivar J, Perez L.F. and Bohoyo F.* Unveiling Powell Basin’s. Tectonic Domains and Understanding Its Abnormal Magnetic Anomaly Signature. Is Heat the Key? // Front. Earth Sci. V. 8:580675. 2020.
https://doi.org/10.3389/feart.2020.580675580675

16. *Chaubey A.K., Dyment J., Bhattacharya G.C., Royer J.Y., Srinivas K., Yatheesh V.* Paleogene magnetic isochrons and palaeo-propagators in the Arabian and Eastern Somali basins, NW Indian Ocean. In: The Tectonic and Climatic Evolution of the Arabian Sea Region. Clift P.D., Croon D., Gaedicke C., Craig J. (Eds.). Geological Society. London. Special Publication. V. 195. P. 71–85. 2002.
17. *Cooper G.R.J, Cowan D.R.* Enhancing potential field data using filters based on the local phase. // Computers & Geoscience. V. 32. P. 1585–1591. 2006. https://doi.org/10.1016/j.cageo.2006.02.016
18. *Cooper G.R.J, Cowan D.R.* A Generalized Derivative Operator for Potential Field Data // Geophysical Prospecting. V. 59. N. 1. P. 188–194. 2011. https://doi.org/10.1111/j.1365-2478.2010.00901.x
19. *DeMets C. and Merkouriev S.* Eurasia-North America Chrons 1-6 plate reconstruction data: Arctic and north Atlantic basins. // MGDS. 2020. https://doi.org/10.1111/j.1365-246X.2008.03761.x
20. *Ferreira F.J.F., de Souza1 J., de B. e S. Bongiolo A. and de Castro L.G.* Enhancement of the total horizontal gradient of magnetic anomalies using the tilt angle // Geophysics. V. 78. N. 3. J33–J41. 2013. https://doi.org/10.1190/geo2011-0441.1
21. *Gay S. P.* Standard curves for the interpretation of magnetic anomalies over long tabular bodies // Geophysics. V. 28. P. 161–200. 1963. https://doi.org/10.1111/j.1365-2478.2010.00901.x
22. *Gradstein F.M., Ogg J.G., Schmitz M.B., Ogg G.M.* Geologic Time Scale 2020. V. 2. Amsterdam. Oxford. Cambridge: Elsevier. 1357 p. 2020.
23. *Gunn P.J.* A Quantitative methods for interpreting aeromagnetic data: a subjective review. // Journal of Australian Geology and Geophysics. V. 17. N. 2. P. 105–113. 1997.
24. *Hey R.* Magnetometer (Geometrics G-882) data as collected during the cruise MGL1309, North Atlantic Seafloor Spreading Geometry Reorganization. // Rolling Deck to Repository (R2R). 2013. https://doi.org/10.7284/112257
25. *Issachar R., Ebbing J. and Dilixiati Y.* New magnetic anomaly map for the Red Sea reveals transtensional structures associated with rotational rifting. // Scientific Report. V.12. Article number 5757. 2022. https://doi.org/10.1038/s41598-022-09770-0
26. *Kumar P., Foufoula-Georgiou E.* Wavelet analysis for geophysical applications // Reviews of Geophysics. V 35. N. 4. P. 385–412. 1997. https://doi.org/10.1029/97RG00427

27. *MacLeod I.N., Jones K. and Dai T.F.* 3-D Analytic Signal in the Interpretation of Total Magnetic Field Data at Low Magnetic Latitudes. // Exploration Geophysics. V. 24. P. 679–688. 1993. https://doi.org/10.1071/EG993679
28. *Miller H.G. and Singh V.* Potential field tilt a new concept for location of potential field sources. // J. Appl. Geophys. V. 32. P. 213–217. 1994. https://doi.org/10.1016/0926-9851(94)90022-1
29. *Merkouriev S. and DeMets C.* A high-resolution model for Eurasia–North America plate kinematics since 20 Ma, // Geophys. J. Int. V. 173. P. 1064–1083. 2008. https://doi.org/10.1111/j.1365-246X.2008.03761.x
30. *Moreau F., Gibert D., Holschneider M., Saracco G.* Wavelet analysis of potential fields. // Inverse Problems. V. 13 N. 1. P. 165–178. 1997.
31. *Nabighian M.N.* The analytical signal of two-dimensional magnetic bodies with polygonal cross-section: its properties and use for automated anomaly interpretation // Geophysics. V. 37, №3. P. 507–517. 1972.
32. *Nabighian M.N.* Additional comments on the analytic signal of two-dimensional magnetic bodies with polygonal cross-section // Geophysics. V. 39. N. 1. P. 85–92. 1974.
33. *Nabighian M.N., Grauch V.J.S., Hansen R.O., Lafehr T.R., Li, Y., Peirce J.W., Phillips J.D., Ruder M.E.* The historical development of the magnetic method in exploration // Geophysics. V. 70. N. 6. P. 33–61. 2005.
34. *Parnell-Turner R., Schouten H. and Smith D.K.* Tectonic Structure of the Mid-Atlantic Ridge near 16◦30'N. // Geochemistry, Geophysics, Geosystems. V. 17. Is. 10. P. 3993-4010. 2016. https://doi.org/10.1002/2016GC006514
35. *Reid A.B., Allsop J.M., Granser H., Millet A.J., and Somerton I.W.* Magnetic interpretation in three dimensions using Euler deconvolution. // Geophysics. V. 55. P. 180–191. 1990. https://doi.org/10.1190/1.1442774
36. *Roest W.R., Verhoef J., and Pilkington M.* Magnetic interpretation using the 3-D analytic signal. // Geophysics. V. 57. P. 116–125 1992.
37. *Saihac P., Galdeano A., Gibert D., Moreau F., Delor C.* Identification of sources of potential fields with the continuous wavelet transform: Complex wavelets and application to aeromagnetic profiles in French Guiana. // JGR Solid Earth. V. 105. Is. B8. P. 19455–19475. 2000. https://doi.org/10.1029/2000JB900090
38. *Salem A, Ravat D, Gamey T.J. and Ushijima K.* Analytic signal approach and its applicability in environmental magnetic investigations. // J. Appl. Geophys. V. 49. P. 231–244. 2002. https://doi.org/10.1016/S0926-9851(02)00125-8

39. *Schouten H., McCamy K.* Filtering marine magnetic anomalies // J. Geophys. Res. V. 77. P. 7089–7099. 1972.
40. *Spector A. and Grant F.S.* Statistical models for interpreting aeromagnetic data. // Geophysics. V. 35. P. 293–302. 1970.
41. *Talwani M. and Heirtzler J.* Computation of magnetic anomalies caused by two dimensional bodies of arbitrary shape / Computers in Mineral Industries, Parks, G.A. Ed. Stanford Univ. Publ. Geol. Sci. V. 9. P. 464–480. 1964.
42. *Thompson D.T.* EULDPH: a new technique for making depth estimates from magnetic data computer-assisted. // Geophysics. V. 47. P. 31–37. 1982.
43. *Verduzco B., Fairhead J.D., Green C.M. and Mackenzie C.* New insights into magnetic derivatives for structural mapping. // Leading Edge. V. 23. P. 116–119. 2004. https://doi.org/10.1190/1.1651454
44. *Wijns C., Pere C. and Kowalczyk P.* Theta map: edge detection in magnetic data. // Geophysics. V. 70. P. L39–L43. 2005.
45. *Werner. S.* Interpretation of magnetic anomalies at sheet_like bodies. // Norstedt. Sveriges Geolologiska Undersok. Ser. C. 1953.

APPENDIX

Summary of formulas for calculating the field of simple bodies and its derivatives.

1.Quadrant

Field

$$B_z = \operatorname{arctg}\left(\frac{x - x_0}{z_1}\right);$$

1st-derivative

$$B_z' = \frac{z_1}{(x - x_0)^2 + {z_1}^2};\ extremum\ in\ x = x_0. \qquad (N1)$$

2nd-derivative

$$B_z'' = \frac{2(x - x_0)z_1}{((x - x_0)^2 + {z_1}^2)^2};\ extrema\ in\ x_\pm = x_0 \pm \frac{\sqrt{3}}{3}\ z_1\ (N2)$$

3rd-я derivative

$$B_z''' = \frac{2z_1(3(x - x_0)^2 - z_1^2)}{((x - x_0)^2 + z_1^2)^3};\ extrema\ in\ x_\pm = x_0 \pm z_1\ (N3)$$

4th-derivative

$$B_z'''' = -\frac{24xz_1((x - x_0)^2 - z_1^2)}{((x - x_0)^2 + z_1^2)^4}$$

2. Plast

Field

$$B_z = \text{arctg}\left(\frac{x-x_0}{z_1}\right) - \text{arctg}\left(\frac{x-x_0}{z_2}\right);\ extrema\ at\ x_{\pm} = \pm\sqrt{z_1 z_2}$$

1-th derivative

$$B_z' = \frac{(z_1 - z_2)(z_1 z_2 - x^2)}{((x-x_0)^2 + z_1^2)((x-x_0)^2 + z_1^2)};$$

$$the\ extrema\ in\ x_{\pm}^1 = x_0 \pm \sqrt{\sqrt{z_1 z_2}\left(z_1 + z_2 + \sqrt{z_1 z_2}\right)}\ (L4),$$

2-th derivative

$$B_z^{"} = \frac{2(x-x_0)z_2}{((x-x_0)^2 + z_2^2)^2} - \frac{2(x-x_0)z_1}{((x-x_0)^2 + z_1^2)^2}$$

$$B_z^{"}(x_{\pm}^1, z_1) = 0 \Rightarrow z_2\left(\left(x_{\pm}^1 - x_0\right)^2 + z_1^2\right)^2 - z_1\left(\left(x_{\pm}^1 - x_0\right)^2 + z_2^2\right)^2 = 0\ (A5)$$

Dyke

$$B_z = \text{arctg}\left(\frac{x-x_0-d}{z_1}\right) - \text{arctg}\left(\frac{x-x_0+d}{z_1}\right)$$

1st-я derivative

$$B_z' = -4z_1 d\,\frac{x-x_0}{[(x-x_0-d)^2 + {z_1}^2][(x-x_0+d)^2 + {z_1}^2]};$$

extrema $x_{\pm} = x_0 \pm \sqrt{\frac{1}{3}}\sqrt{2\sqrt{d^4 + d^2 z_1^2 + z_1^4} + d^2 - z_1^2}\ (N6)$

2nd-derivative

$$B_z^{"} = \frac{2(x-x_0+d)z_1}{[(x-x_0+d)^2 + z_1^2]^{2-2}} - \frac{2(x-x_0-d)z_1}{[(x-x_0-d)^2 + z_1^2]^2}\ (N7)$$

3rd-derivative

$$4B_z^{"\prime} = {}^{p}/_{q}\ \ (N8)$$

$$,where$$

$$p = 16xdz_1(-3x^6 + 3x^4 d^{2-3} - 3x^4 z_1^2 + 3x^2 d^2 + 14x^2 d^2 z_1^2 + 3x^2 z_1^{4-3} - 3d^{6-3} - 3d^4 z_1^2 + 3d^2 z_1^4 + 3z_1^6)$$

$$q = (x^2 - 2xd + d^2 + z_1^2)^3 (x^2 + 2xd + d^2 + z_1^2)^3$$

Block

Field

$$B_z = \text{arctg}\left(\frac{x - x_0 - d}{z_2}\right) + \text{arctg}\left(\frac{x - x_0 + d}{z_1}\right) - \text{arctg}\left(\frac{x - x_0 - d}{z_1}\right) - \text{arctg}\left(\frac{\mathrm{x} - \mathrm{x}_0 + \mathrm{d}}{\mathrm{z}_2}\right)$$

1st derivative

$$B_z' = \frac{z_1}{(x - x_0 - d)^2 + {z_1}^2} - \frac{z_2}{(x - x_0 - d)^2 + {z_2}^2} - \frac{z_1}{(x - x_0 + d)^2 + {z_1}^2} + \frac{z_2}{(x - x_0 + d)^2 + {z_2}^2}$$

The analytical expression for the extrema-of the 1st derivative (zeros-of the 2nd) is not given due to its cumbersomeness

2nd-derivative

$$B_z'' = \frac{2(x - x_0 - d)z_2}{[(x - x_0 - d)^2 + z_2^2]^{2-2}} - \frac{2(x - x_0 - d)z_1}{[(x - x_0 - d)^2 + z_1^2]^2} + \frac{2(x - x_0 + d)z_1}{[(x - x_0 + d)^2 + z_1^2]^2} - \frac{2(x - x_0 + d)z_2}{[(x - x_0 + d)^2 + z_2^2]^2}$$

Table1. Coordinates of block centers before and after correction

Block center positions *xc*	xc_1, km	xc_2, km	xc_3, km
Set	-5.5	-0.5	5
By the extrema *of the Bz field*	-5.930	-0.557	5.550
By1-the 1st derivative	-6.147147	-0.557557	5.590
By-the 3rd derivative	-5.756	-0.497	5.263
After correction	-5.482	-0.506	4.984

Table 2. Block half-widths before and after correction

Half-widths	*of blocks*$_{d1}$, km	*, km*$_{d2}$, km	*d*,km d3, km
Given	4.5	0.5	5
Obtained from the 3rdfrom the 3rdderivative	4.236	1.023	4.7365
At step 1	4.136	0.582	4.657
After correction	4.443	0.575	4.956

FIGURE CAPTIONS

Figure 1. Geometry and parameters of 2D geophysical models. (*a*) –quadrant, semi-infinite vertically and horizontally body; (*b*– - formation, semi-infinite horizontally layer; (*в*с – - dike; (*d*) - block.

2. Waveletspectra of the quadrant field for three Gaussian functions. (*a*) – *m* = 1*,* (*b*) – *m* = *2*, and *(в*с) – *m* = 3, respectively. Continuous lines represent the isolines of the coefficients of the wavelet spectrum, and points represent the positions of local maxima onpa fixed scale.

Fig. 3. Errors in determining the depth and thickness of the reservoirfrom the 3rdderivative. (*a*) – error in determining the depth, symbols show the dependence on the thickness *h* in km: *h* = 0.5–●, *h* = 1–◆, *h* = 2 – ▲, *h* = 3–■, *h* = 4–○, *h* = 6 – ◇, *h* = 7–△, *h* = 8–□; (*b*) – error in determining the thickness, symbols show the dependence on z_1z1 in km:z_1 = z1 = 1–●, z1 z_1 = 2–▲, z_1 z1 = 4 – ◆; (*b*) - relative error in determining the thickness in dimensionless units.

Рис. 4. Error in determining the depth and half-width of the dike from the extrema-of the 3rd derivative. (*a*) – $error_{\text{in determining}}$z1; (*b*) – error in determining half – width; (*в*с) – the same as (*a*) after correction; (*d*) - the same as (*b*) after correction; the characters on (*a*) and (*в*с) correspond to different half-widths, on (*b*) and (*d*) – dike depths.

Figure 5. Comparison of the interpretation capabilities of the wavelet method and метода the analytical signal method. The solid line shows the theoretical dependence for the wavelet method, the dashed line shows the 1st one for the analytical signal, the triangles show the values obtained from the extrema of the derivative, and the circles show the same values for the extrema-of the 3rd derivative.

Figure 6. The field created by the structure of 3 blocks, its derivatives and the result of interpretation. A bold black line shows the field, a long dashed line shows the 1st derivative, a short dashed line shows the 2nd derivative, and a solid gray line shows the 3rd derivative. (*a*) the specified structure, (*b*) the initial estimate, and (*в*с) after correction.

Figure 7. Comparison of two methods for determining the boundaries of anomaly sources for the spreading model. (*a*) –magnetic anomalies calculated from the spreading model, dark rectangles show blocks of direct polarity, alphanumeric symbols – границы chronboundaries; (*b*) - analytical signal; (*в*с – - comparison of the position of the chron boundaries: otrezki с ▲– the desired boundaries of bodies, otrezki с ▼- found with the help of wavelet analysis, opoints с ◆-found using an analytical signal; (*d*) - wavelet transform, isolines show the modulus of wavelet coefficients, and a broken line shows local extrema.

Figure 8. Magnetometric profile crossing the Reikjanes ridge Рейкъянесin the North Atlantic. *a*) – рельефа дна; (*б*(a – - bottom relief; (b) - magnetic anomalies measured on the KNOR24 profile,

symbols – chrones; numbers – numbers of the main anomalies; (*вс*) - shadow map of the bottom relief with the positions of isochrons and observed magnetic anomalies taken out onthe KNOR24 magnetometric profile, symbols are the same as on (*b*).

Figure 9. Comparison of two methods for determining the boundaries of sources of magnetic anomalies for the KNOR24 profile. (*a*) – magnetic anomalies observed on the profile, dark rectangles show blocks of direct polarity, alphanumeric symbols – chron boundaries; (*b*) - analytical signal; (*вс* – - comparison of the position of the chron boundaries; (*d*) is a wavelettransform. The symbols are the same as for Figure 7.

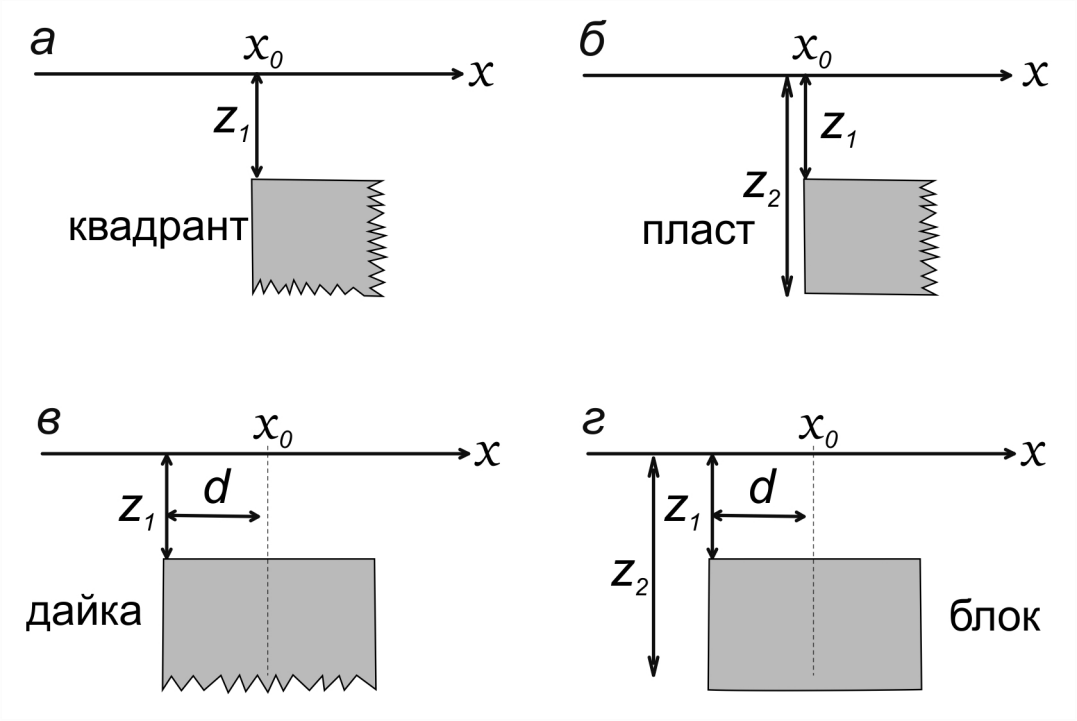

Figure 1.

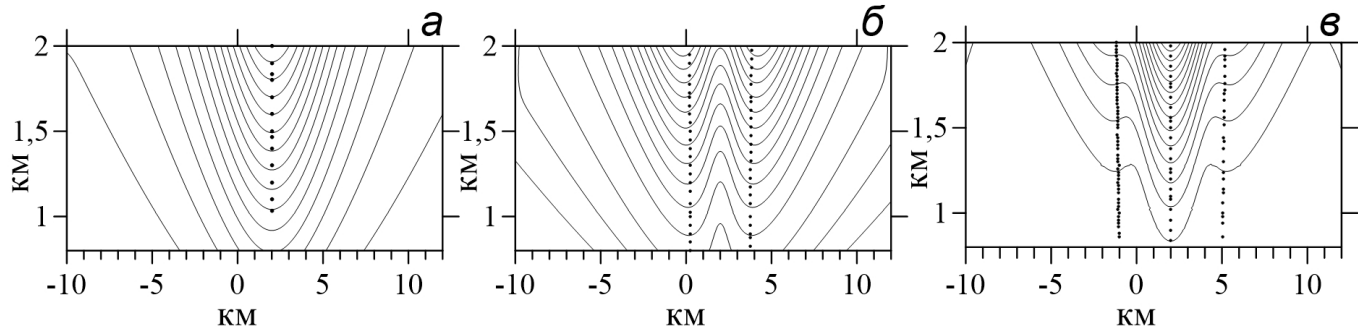

Figure 2.

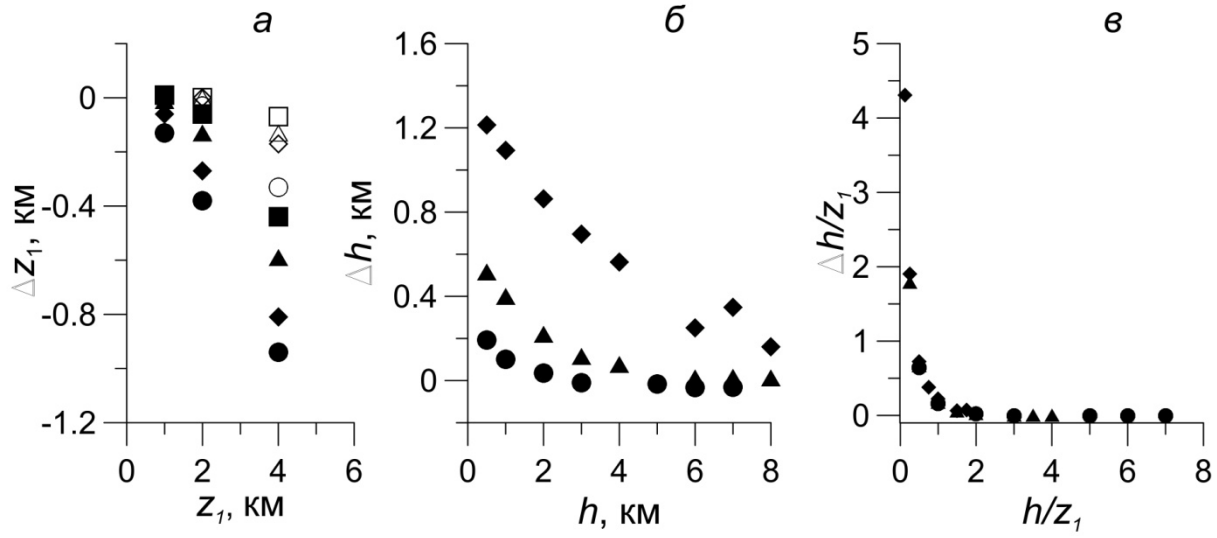

Figure 3..

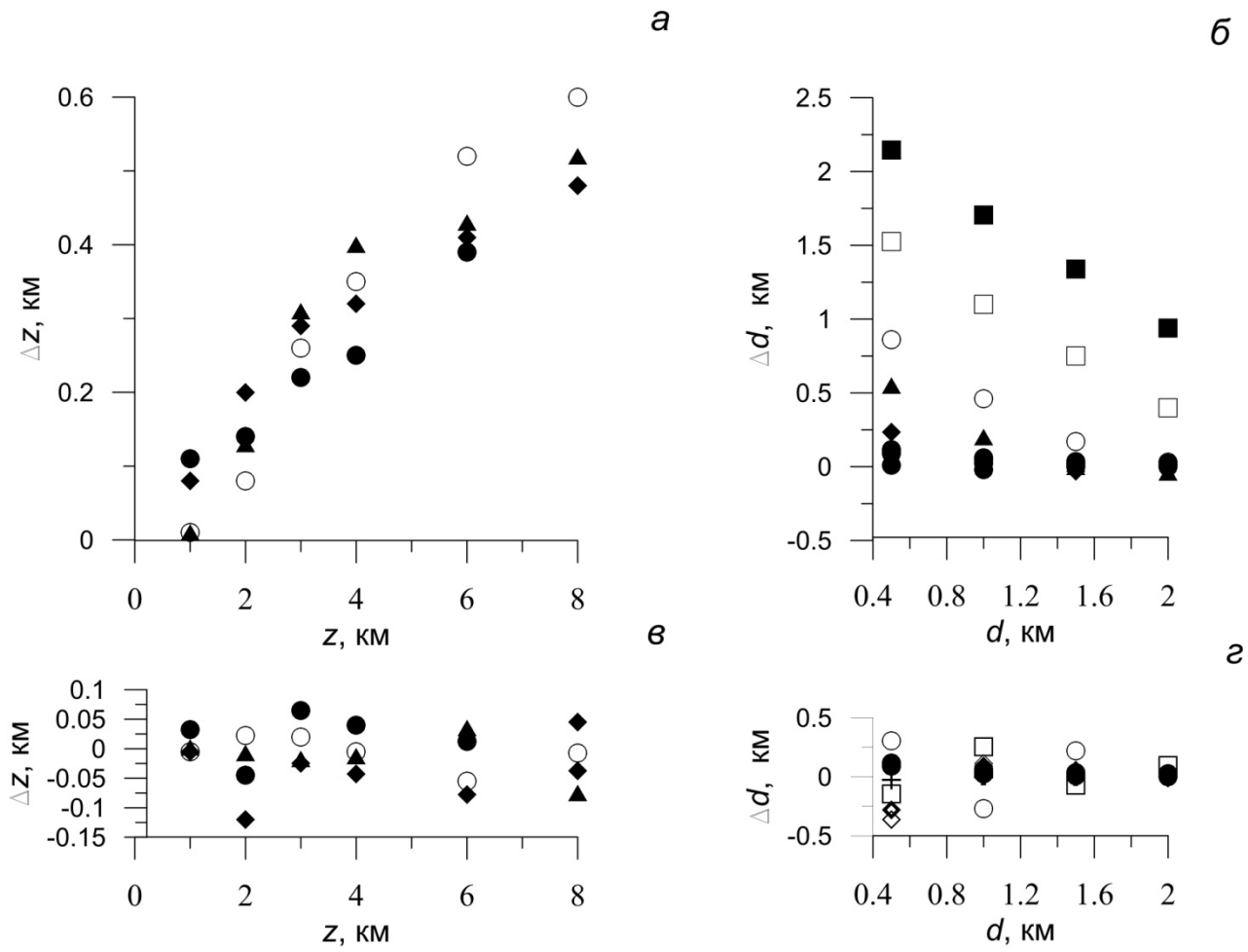
а
б
в
г
0.6
0.4
0.2
0
△z, км
0
2
4
6
8
z, км
2.5
2
1.5
1
0.5
0
-0.5
△d, км
0.4
0.8
1.2
1.6
2
d, км
0.1
0.05
0
-0.05
-0.1
-0.15
△z, км
0
2
4
6
8
z, км
0.5
0
-0.5
△d, км
0.4
0.8
1.2
1.6
2
d, км

Figure 4.

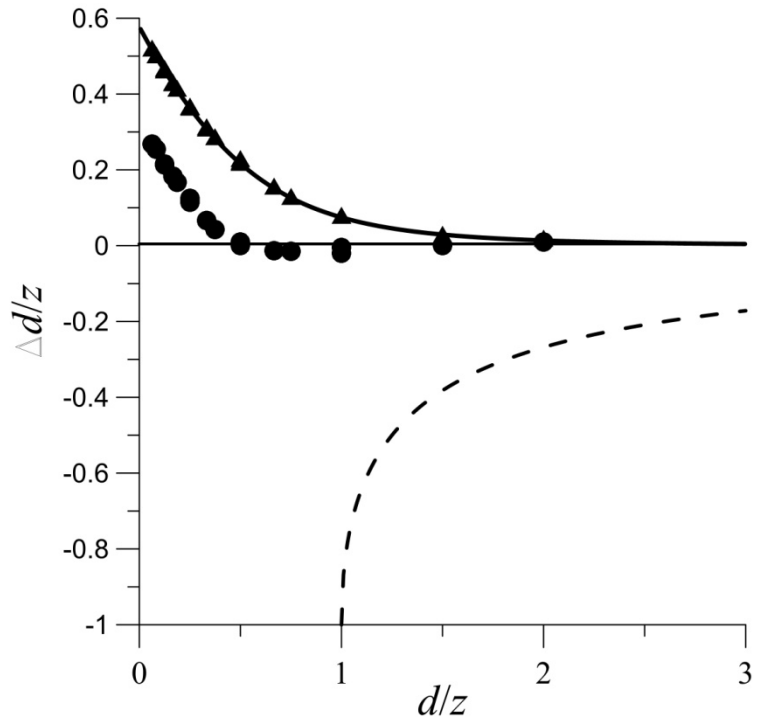

Figure 5.

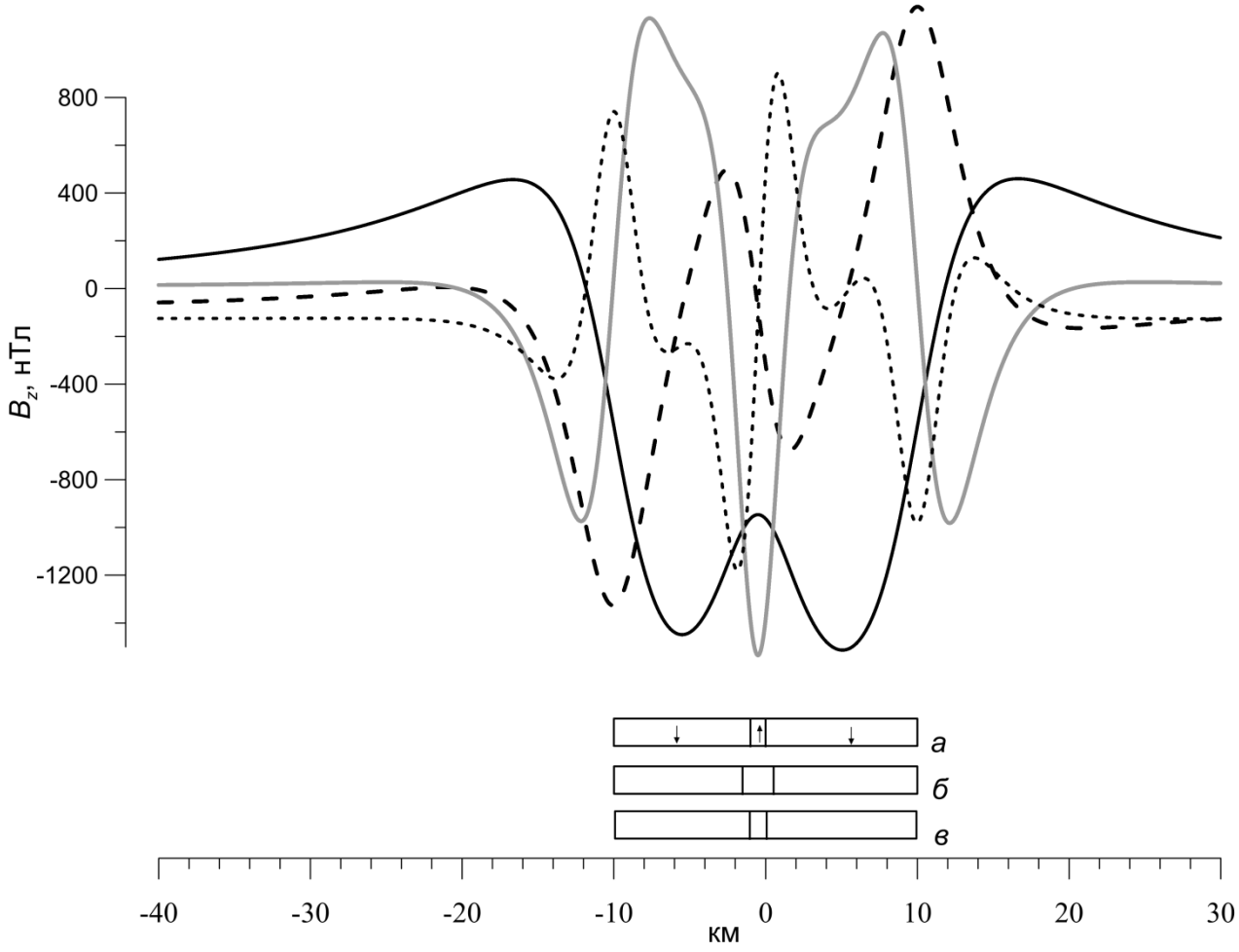

Figure 6.

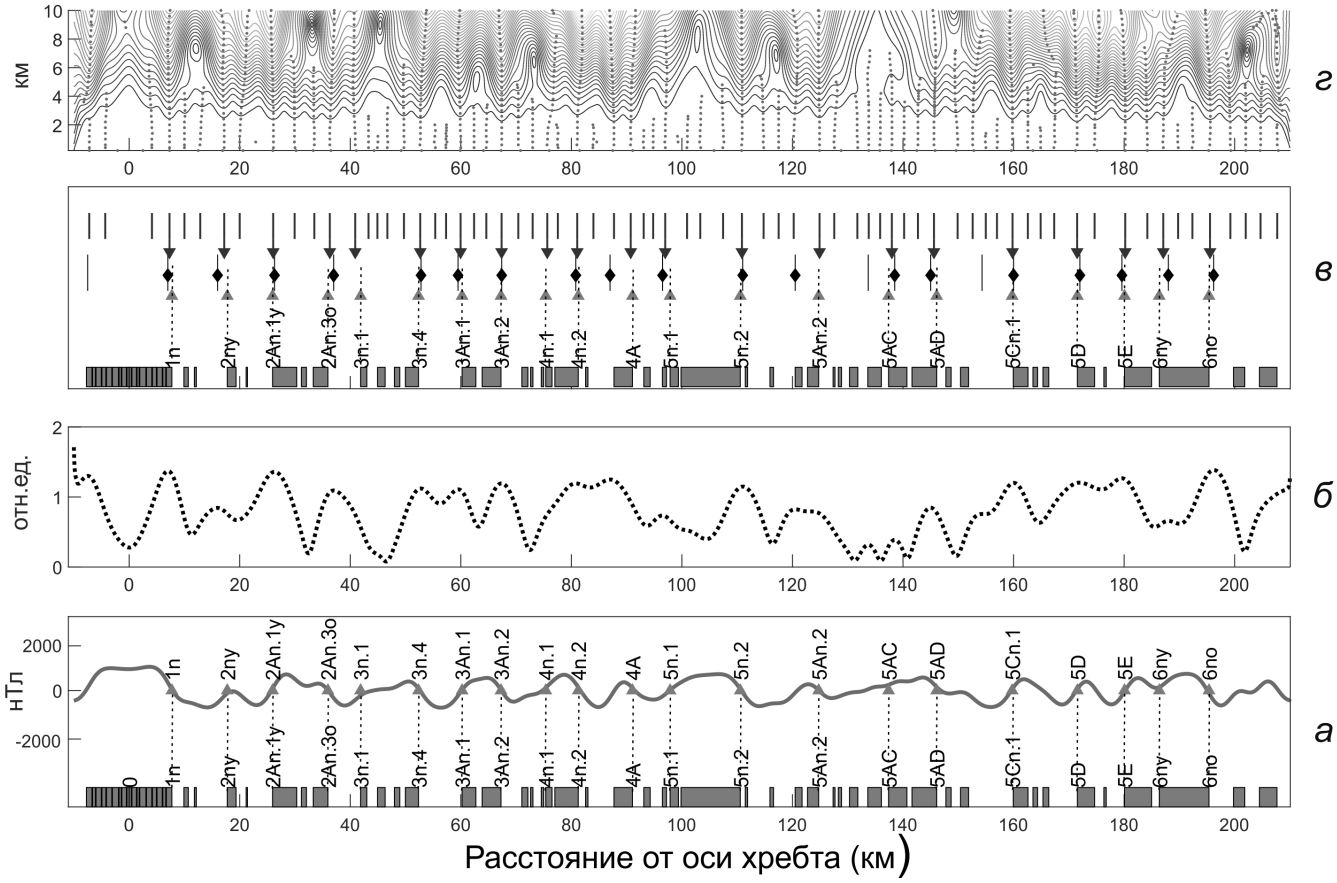
км
г
в
отн.ед.
б
нТл
а
1n
2ny
2An.1y
2An.3o
3n.1
3n.4
3An.1
3An.2
4n.1
4n.2
4A
5n.1
5n.2
5An.2
5AC
5AD
5Cn.1
5D
5E
6ny
6no
Расстояние от оси хребта (км)

Figure 7.

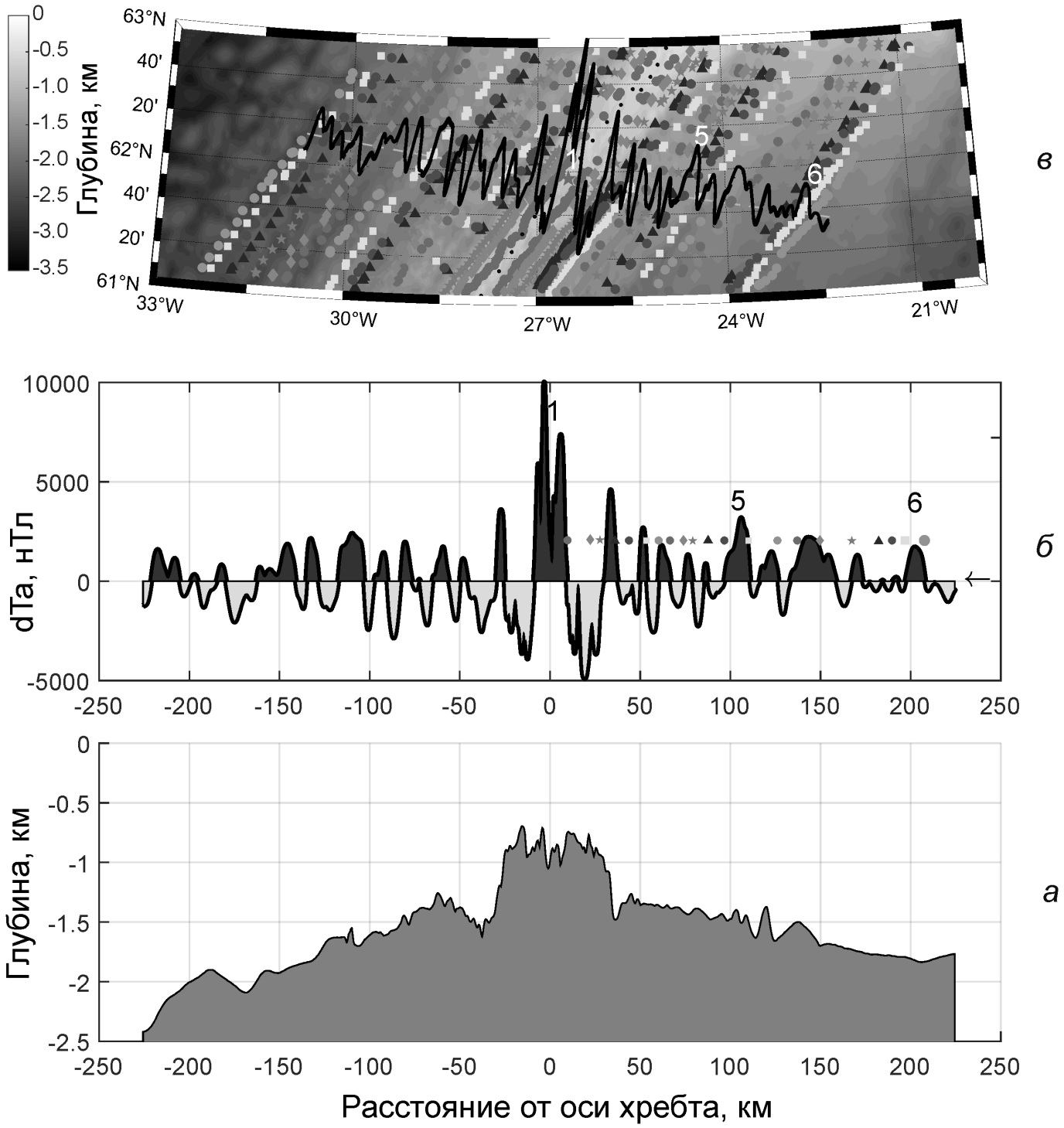
0
-0.5
-1.0
-1.5
-2.0
-2.5
-3.0
-3.5
Глубина, км
63°N
40'
20'
62°N
40'
20'
61°N
33°W
30°W
27°W
24°W
21°W
1
5
6
в
10000
5000
0
-5000
dTa, нТл
-250
-200
-150
-100
-50
0
50
100
150
200
250
1
5
6
б
0
-0.5
-1
-1.5
-2
-2.5
Глубина, км
а
Расстояние от оси хребта, км

Figure 8.

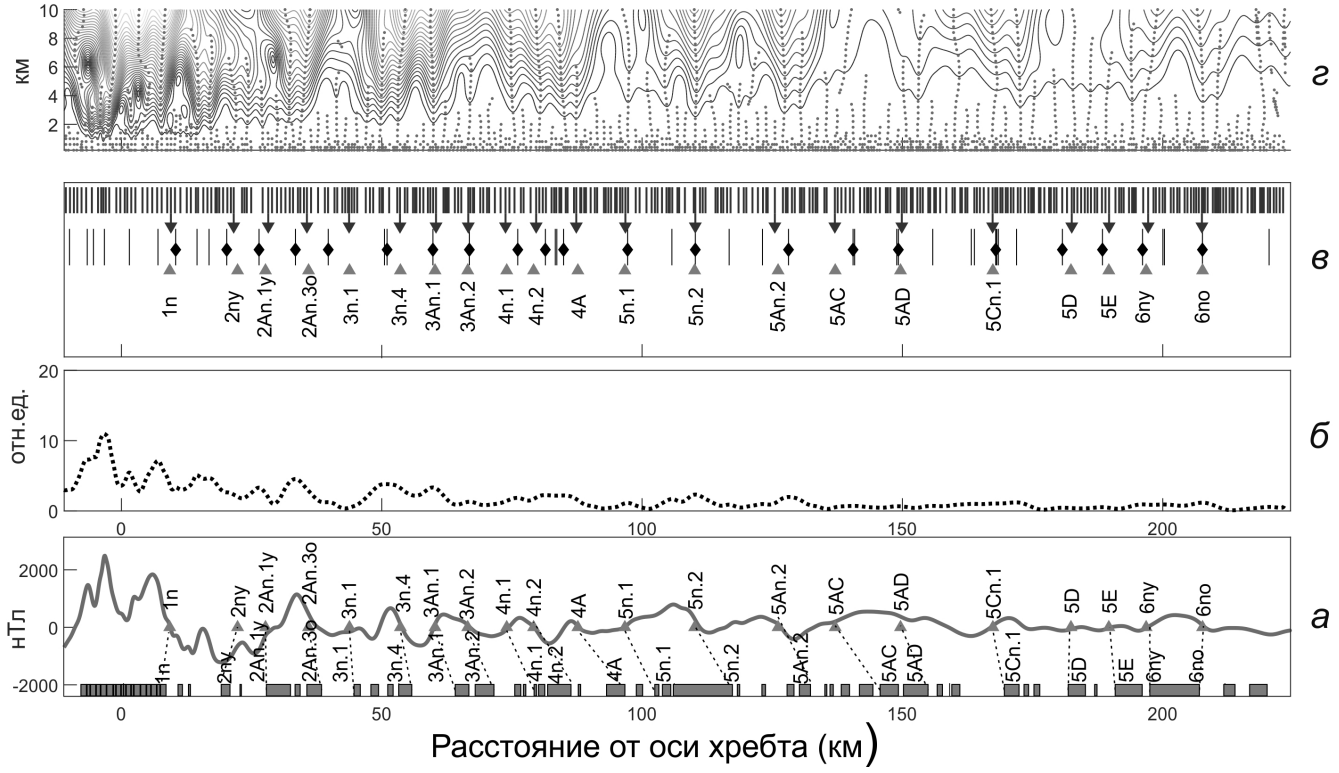
км
г
в
1n
2ny
2An.1y
2An.3o
3n.1
3n.4
3An.1
3An.2
4n.1
4n.2
4A
5n.1
5n.2
5An.2
5AC
5AD
5Cn.1
5D
5E
6ny
6no
отн.ед.
б
нТл
а
Расстояние от оси хребта (км)

Figure 9.